In situ doping control of the surface of high-temperature superconductors

M. A. HOSSAIN[1]*, J. D. F. MOTTERSHEAD[1]*, D. FOURNIER[1], A. BOSTWICK[2], J. L. McCHESNEY[2], E. ROTENBERG[2], R. LIANG[3], W. N. HARDY[1,3], G. A. SAWATZKY[1,3], I. S. ELFIMOV[3], D. A. BONN[1,3] AND A. DAMASCELLI[1,3]†

[1]Department of Physics and Astronomy, University of British Columbia, Vancouver, British Columbia V6T 1Z1, Canada
[2]Advanced Light Source, Lawrence Berkeley National Laboratory, Berkeley, California 94720, USA
[3]AMPEL, University of British Columbia, Vancouver, British Columbia V6T 1Z4, Canada
*These authors contributed equally to this work
†e-mail: damascelli@physics.ubc.ca

Central to the understanding of high-temperature superconductivity is the evolution of the electronic structure as doping alters the density of charge carriers in the CuO_2 planes. Superconductivity emerges along the path from a normal metal on the overdoped side to an antiferromagnetic insulator on the underdoped side. This path also exhibits a severe disruption of the overdoped normal metal's Fermi surface[1–3]. Angle-resolved photoemission spectroscopy (ARPES) on the surfaces of easily cleaved materials such as $Bi_2Sr_2CaCu_2O_{8+\delta}$ shows that in zero magnetic field the Fermi surface breaks up into disconnected arcs[4–6]. However, in high magnetic field, quantum oscillations[7] at low temperatures in $YBa_2Cu_3O_{6.5}$ indicate the existence of small Fermi surface pockets[8–18]. Reconciling these two phenomena through ARPES studies of $YBa_2Cu_3O_{7-\delta}$ (YBCO) has been hampered by the surface sensitivity of the technique[19–21]. Here, we show that this difficulty stems from the polarity and resulting self-doping of the YBCO surface. Through *in situ* deposition of potassium atoms on cleaved YBCO, we can continuously control the surface doping and follow the evolution of the Fermi surface from the overdoped to the underdoped regime. The present approach opens the door to systematic studies of high-temperature superconductors, such as creating new electron-doped superconductors from insulating parent compounds.

In the heavily overdoped regime, angular magnetoresistance oscillation[1] and angle-resolved photoemission spectroscopy (ARPES) experiments[2,3] on $Tl_2Ba_2CuO_{6+\delta}$ have arrived at a quantitative consensus in observing a large hole-like Fermi surface. On reducing the number of holes in the CuO_2 planes, the Fermi surface volume decreases in the manner expected by Luttinger's theorem, but below optimal doping the single-particle Fermi surface seems to reduce to four disconnected nodal Fermi arcs. This scenario was suggested from ARPES studies of Bi cuprates[4,5] and $Ca_{2-x}Na_xCuO_2Cl_2$ (ref. 6), and is thought to be connected to the existence of the pseudogap. The detection of quantum oscillations in oxygen-ordered ortho-II $YBa_2Cu_3O_{6.5}$ (YBCO6.5) suggests a different scenario involving Fermi surface reconstruction into hole and/or electron pockets[7,9,10]. These two pictures are derived from quite different measurement techniques, carried out on different materials, and under conditions of high magnetic field in one case, but zero field in the other. Owing to the complex multiband
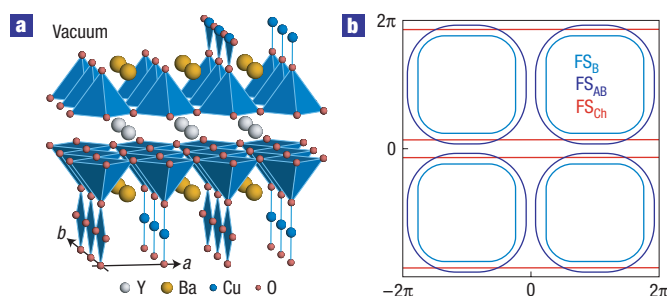

Figure 1 The surface of cleaved YBCO. a, Crystal structure of oxygen-ordered YBCO6.5 (with alternating oxygen-full and -empty chains), showing the BaO-plane and CuO-chain terminations of the cleaved surface. Electronic reconstruction takes place at these polar surfaces, similar to the prototypical case of a polar catastrophe in ionic insulators with a $|1+|1-|1+|1-|\dots$ layer-by-layer charge[25]. **b**, This leads to larger-than-expected Fermi surface features for the surface topmost layers: the one-dimensional CuO-chain band (FS_{Ch}) and especially 'overdoped-like' CuO_2-plane bonding and antibonding bands (FS_B and FS_{AB}).

and correlated character of the electronic structure of YBCO6.5 (ref. 11), the determination of the nature of these pockets and their generality to the underdoped cuprates requires connecting transport and single-particle spectroscopy information on the same underdoped system. The study of YBCO6.5 by ARPES is thus crucial. Unfortunately, this material is complicated by the lack of a natural [001] cleavage plane (Fig. 1a) and also by the presence of CuO-chain layers. More specifically, YBCO cleaves between the CuO-chain layer and the BaO layer, leaving on the cleaved surface relatively large regions (>100 Å) of either CuO or BaO terminations. Scanning tunnelling microscopy shows that the CuO-chain terraces are characterized by prominent surface density waves[22] and differ substantially from the bulk: as also seen in ARPES[19], they exhibit surface states and unavoidable doping disorder. Recent ARPES studies of nearly optimally doped YBCO indicated that surfaces terminating in either a CuO and BaO layer give different contributions to the total photoemission intensity[21],
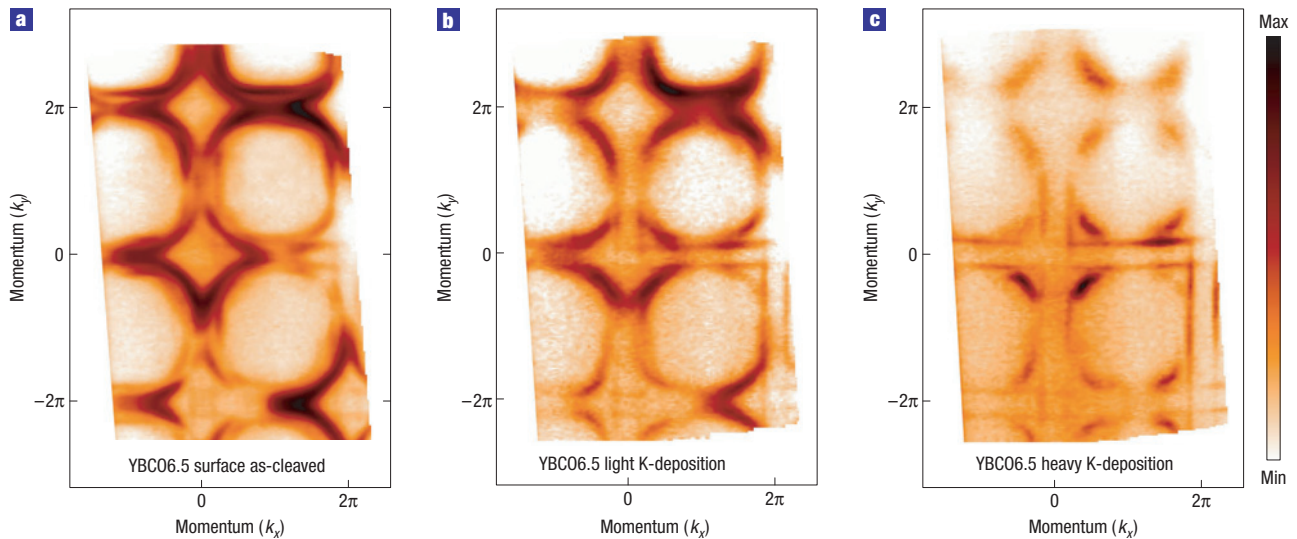
Figure 2 YBCO Fermi surface evolution on electron doping. a, ARPES Fermi surface of as-cleaved YBCO6.5, exhibiting an effective hole doping $p = 0.28$ per planar Cu atom, as determined from the average area of bonding and antibonding CuO$_2$-bilayer Fermi surfaces. **b,c**, By evaporating potassium on the same sample (<1 monolayer), electrons are transferred to the topmost CuO$_2$ bilayer and the corresponding Fermi surfaces become progressively more hole-underdoped; for heavy K-deposition ($p = 0.11$ as estimated from the area of the chain Fermi surface), the E_F ARPES intensity reduces to the 1D CuO-chain Fermi surface and four disconnected nodal CuO$_2$ Fermi arcs (**c**).

and that the doping of the topmost CuO$_2$ planes is $p = 0.3$, almost irrespective of the nominal bulk doping. This corresponds to heavy overdoping, all the way into the non-superconducting regime (Fig. 4), and is actually not achievable in bulk, fully oxygenated YBCO7.0 for which $p = 0.194$ (ref. 23). Similar problems have been encountered in the ARPES study of YBa$_2$Cu$_4$O$_8$ (ref. 24).

Overcoming these problems requires, first of all, recognizing that the cleaved surface of YBCO is actually polar. This can lead to overdoped-like Fermi surfaces (Fig. 1b) due to reconstruction of the electronic states[25]. A wide momentum-distribution map of the Fermi surface from 'as-cleaved' YBCO6.5 is shown in Fig. 2a (see the Methods section). The ARPES data are a superposition of features from the BaO- and CuO-terminated regions: because of the few ångström electron escape depth at these photon energies, the ARPES intensity from the BaO-terminated regions is dominated by the CuO$_2$-bilayer bands and that from the CuO-terminated regions by the chain band. The comparison with Fig. 1b enables us to identify the Fermi surface features originating from the CuO$_2$-plane bonding and antibonding bands (FS$_B$ and FS$_{AB}$) and the one-dimensional (1D) CuO-chain band (FS$_{Ch}$). Note that the strong momentum-dependent intensity modulation of the ARPES features, which seems inconsistent with the sample symmetry, is simply a manifestation of the matrix element effects associated with the photon/crystal/electron geometry changing across the field of view (no symmetrization was carried out). In addition, this particular ortho-II sample happened to be twinned, in the bulk and not just on the surface, as confirmed by X-ray diffraction (this has an effect on FS$_{Ch}$ but not on the discussion of the four-fold symmetric Fermi arcs). Most importantly, the fit of the 2D ARPES Fermi surfaces over multiple zones returns the following areas, counting electrons, relative to the Brillouin zone area $A_{BZ} = 4\pi^2/ab$: the bonding Fermi surface area FS$_B = 46.2\%$, the antibonding FS$_{AB} = 26.0\%$ and the chain surface FS$_{Ch} = 13.8\%$. From the average of bonding and antibonding Fermi surface areas, we can calculate the hole doping $p = 0.28 \pm 0.01$ per planar copper ($p = 0$ for the 1/2-filled Mott insulator with 1 hole per Cu atom). As summarized in the phase diagram of Fig. 4, this indicates that

the self-doping of the YBCO6.5 polar surface is that of a heavily overdoped, non-superconducting cuprate.

The next step is that of actively controlling the self-doping of the surface, to reduce its hole content to that of underdoped, bulk YBCO6.5. This can be achieved by *in situ* evaporation of potassium onto the cleaved surface (see the Methods section): owing to the low ionization potential, K^{1+} ions are adsorbed on the surface and electrons are doped into the topmost layers. As a consequence, we would anticipate the evolution of all detected features towards the underdoped regime of hole-doped cuprates, which is precisely what can be observed in Fig. 2, from a to c, on increasing the K^{1+} concentration (decreasing the hole doping). The doping is indeed changing according to an increase in electron filling (all data were acquired on the same sample after subsequent K evaporations). This is demonstrated by the continuous FS$_{Ch}$ area increase (counting electrons), which evolves from FS$_{Ch} = 13.8\%$ for the as-cleaved surface to FS$_{Ch}^{K1} = 14.7\%$ and FS$_{Ch}^{K2} = 16.6\%$ for the increasingly K-deposited YBCOK1 (Fig. 2b) and YBCOK2 (Fig. 2c). By comparing the carrier concentration per chain Cu measured by the FS$_{Ch}$ area with the results of *ab initio* local density approximation (LDA) band-structure calculations[11], we can estimate the corresponding hole doping per planar Cu. This way we find good agreement with the value $p = 0.28$ already estimated for as-cleaved YBCO6.5 from the average of FS$_B$ and FS$_{AB}$. Most importantly, however, we obtain a hole doping $p^{K1} = 0.20$ and $p^{K2} = 0.11$ for YBCOK1 and YBCOK2, which means that the surface of YBCOK$_2$ is very close to the doping level $p = 0.097$ of bulk oxygen-ordered ortho-II YBCO6.5.

The most interesting aspect of the data in Fig. 2 is the evolution of the CuO$_2$-plane features. For heavy K deposition (Fig. 2c), the LDA-like CuO$_2$-bilayer bonding and antibonding Fermi surfaces of overdoped YBCO have collapsed into four nodal Fermi arcs, consistent with other underdoped cuprates[4–6]. This is accompanied by the complete suppression of CuO$_2$ antinodal spectral intensity as well as nodal bilayer splitting, which in contrast were clearly resolved for as-cleaved YBCO6.5 (Fig. 2a). Their disappearance with K deposition suggests a severe loss of coherence
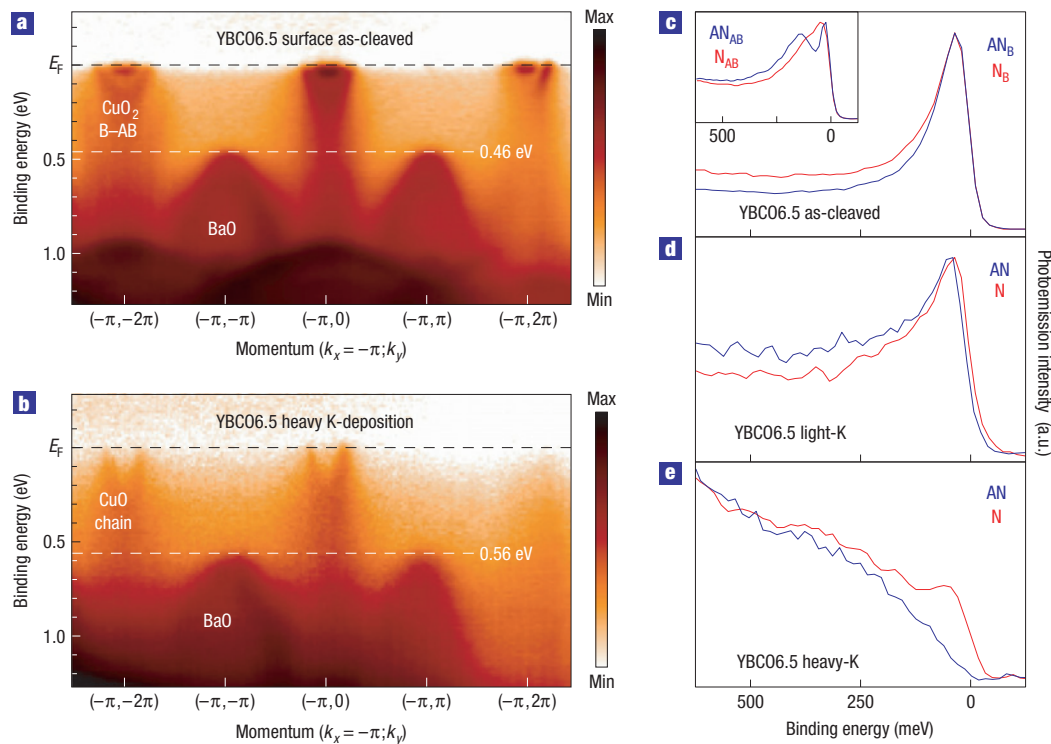
Figure 3 YBCO dispersion and EDC evolution on electron doping. a,b, The BaO-band high-energy shift in YBCOK2 as compared with YBCO6.5 reveals that electrons are added on K deposition; in addition, bonding (B) and antibonding (AB) CuO_2 features vanish at the antinodes and only the CuO-chain band is detected. **c–e,** Nodal (N) and antinodal (AN) k_F EDCs showing the progressive opening of an antinodal gap and loss of CuO_2-plane quasiparticle coherence on underdoping ($\Delta \sim 10$ and 80 meV for YBCOK1 and YBCOK2); the bonding (**c**) and antibonding (**c**, inset) splitting is resolved only for as-cleaved YBCO6.5.

on underdoping. Correspondingly, the CuO_2 nodal Fermi wave vectors, relative to the Brillouin zone diagonal $(0,0)–(\pi,\pi)$, have evolved from $k_F^{AB} = 0.29$ and $k_F^B = 0.36$ for 'overdoped' as-cleaved YBCO6.5, to a single $k_F^{K2} = 0.40$ for 'underdoped' YBCOK2. These numbers compare well to what has been observed on other cuprates at similar dopings (note that the following are both single CuO_2-layer systems): $k_F = 0.36$ and 0.41, respectively, for overdoped ($p = 0.26$) $Tl_2Ba_2CuO_{6+\delta}$ (ref. 2) and underdoped ($p = 0.12$) $Ca_{2-x}Na_xCuO_2Cl_2$ (ref. 6).

The transfer of electrons to the surface of YBCO on K deposition is also confirmed by an inspection of the electronic dispersions along the $(-\pi, -2\pi)–(-\pi, 2\pi)$ direction (corresponding momentum-distribution curves are shown in the Supplementary Information). On $p = 0.28$ as-cleaved YBCO6.5 (Fig. 3a), we detect well-defined bonding and antibonding CuO_2 bands crossing E_F at the antinodes, as well as the BaO band with a maximum binding energy at the zone corners $(-\pi, \pm\pi)$. On underdoped $p = 0.11$ YBCOK2 (Fig. 3b), the BaO band is located $\sim$100 meV deeper in energy. This indicates a shift of the chemical potential consistent with the transfer of electrons from adsorbed K atoms to the topmost BaO-plane, CuO-chain and CuO_2-plane layers. On YBCOK2, the only coherent feature detected at the antinodes is the 1D CuO-chain band; the antinodal CuO_2-plane spectral weight has now become fully incoherent. The nodal and antinodal energy-distribution curves (EDCs) in Fig. 3c–e clearly show that the progressive loss of quasiparticle coherence with K deposition is very similar to what is observed on other cuprates on hole underdoping[2,4–6]. Most importantly, whereas metallic behaviour is observed on as-cleaved YBCO6.5, a leading-edge antinodal gap $\Delta \sim 10$ and 80 meV is detected

for YBCOK1 and YBCOK2, respectively. This is consistent with YBCO being superconducting for $p = 0.11$ and 0.20 but not 0.28 (Fig. 4—the experiments were all carried out at $T = 20$ K), and enables us to conclude that the properties of the K-deposited YBCO surfaces are representative of bulk YBCO.

We now summarize our findings, illustrated by the phase diagram and symmetrized Fermi surface data for YBCOK2 and as-cleaved YBCO6.5 in Fig. 4. Our study demonstrates that the self-hole-doping of the cleaved polar surfaces of YBCO can be controlled by the *in situ* evaporation of alkali metals, in the present case K. This novel approach paves the way for the study of this important material family—across the whole phase diagram—by single-particle spectroscopies. As this material has been the gold standard in a number of seminal bulk-sensitive studies of the normal and superconducting properties, the direct connection with single-particle spectroscopy can lead to an understandable underdoped anchor point, analogous to $Tl_2Ba_2CuO_{6+\delta}$ in the overdoped regime[3]. The results obtained for $p = 0.11$ YBCOK2 establish that the ARPES Fermi surface of underdoped YBCO consists of the superposition of 1D CuO-chain Fermi surface and CuO_2-plane-derived nodal Fermi arcs. It is thus consistent, with the extra complication of the chains, to what has already been observed in oxychloride[6] and Bi cuprates[4,5]. In this sense, the disruption of the large hole-like coherent Fermi surface in underdoped cuprates is a truly universal phenomenon.

Having obtained the first momentum-resolved Fermi surface data for underdoped YBCO, it becomes crucial to understand the connection between ARPES and quantum oscillation results[7,10]. First, the detection of the BaO-band maximum at $\sim$0.5 eV below E_F rules out the scenario coming from LDA band-structure
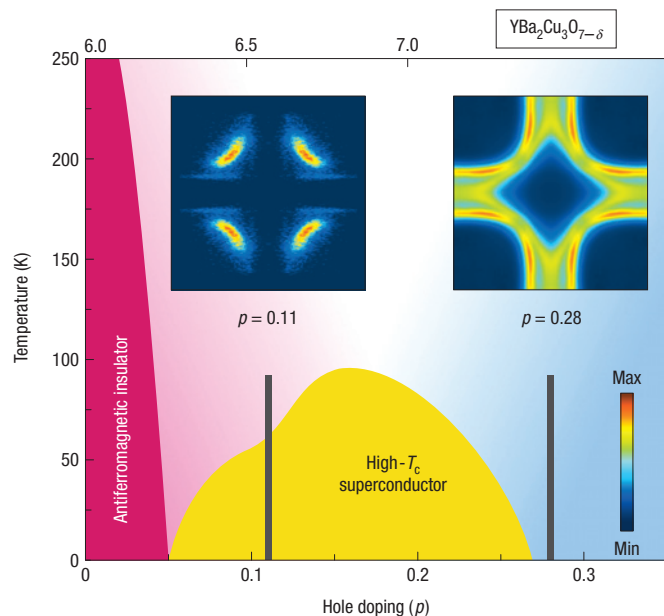
Figure 4 Phase diagram of YBCO by ARPES. Schematic temperature-doping phase diagram of YBCO adapted from ref. 7. The hole doping p per planar copper ($p = 0$ for the 1/2-filled Mott insulator with 1 hole per Cu atom), and the corresponding oxygen content ($7 - \delta$), are indicated on the bottom and top axes[23]. The ARPES Fermi surface for under- and overdoped YBCO is also shown; the momentum-distribution maps have been two-fold and four-fold symmetrized for $p = 0.11$ and 0.28, respectively. Similar to the data in Fig. 2, the doping levels were determined for $p = 0.11$ from the area of FS_{Ch}, and for $p = 0.28$ from the area of FS_B and FS_{AB}.

calculations, which suggested that the small Fermi surface found in the quantum oscillation measurements might originate from small pockets produced by BaO–Cu$_{chain}$ bands at $(\pm\pi, \pm\pi)$[11,12]. We also did not observe any signature of CuO$_2$-derived band folding arising from the ortho-II oxygen-ordering of the chains[11,12], which is possibly consistent with the loss of three-dimensional coherence demonstrated by the suppression of bilayer band splitting on underdoping. Recent measurements of the Hall resistance in high magnetic field have noted a sign change with decreasing temperature[9], suggesting that the quantum oscillations seen on top of a negative Hall coefficient might come from small electron pockets, rather than the hole pockets originally proposed[7]. However, there is no sign of such electron pockets in our ARPES data from underdoped YBCOK2, nor are there signs of extra zone-folding due to the kinds of density wave instabilities that might give rise to such a Fermi surface reconstruction[8,9,15].

If any pocket had to be postulated on the basis of the present ARPES data, the most obvious possibility would be that the Fermi arcs are in fact hole-like nodal Fermi pockets, as obtained for light doping of the antiferromagnetic parent compound in self-consistent Born calculations[26] and already speculated from the study of other underdoped cuprates[4–6]. The lack of a finite ARPES intensity on the outer side of the pockets would be consistent with the strong drop in the quasiparticle coherence $Z_\mathbf{k}$ expected beyond the antiferromagnetic zone boundary[13,27]. To estimate an area for these ostensible nodal pockets, we can fold the detected arc profile, either with respect to the antiferromagnetic zone boundary or the end points of the arc itself, obtaining values of either 2.6% or 1.3%, relative to the full Brillouin zone area $A_{BZ} = 4\pi^2/ab$. These numbers compare relatively well to the pocket area of 1.9% suggested on the basis of quantum oscillation experiments on

bulk YBCO6.5 (refs 7,10). However, these are hole, not electron pockets. Thus, the interpretation of high field measurements in terms of electron and hole pockets differs markedly from single-particle spectroscopy on the same material, suggesting that the high magnetic field might be inducing a state different from that being studied in zero field.

Whatever the solution to the puzzle outlined above, it should be emphasized that the present approach, based on the *in situ* alkaline metal evaporation on freshly cleaved surfaces, opens the door to this type of manipulation of other cuprates and complex oxides, not only to control the self-doping of polar surfaces but also to reach doping levels otherwise precluded in the bulk. For instance, we could try to underdope the surface of Tl$_2$Ba$_2$CuO$_{6+\delta}$, which grows naturally overdoped[3], or even to obtain an electron-doped superconductor starting from the insulating parent compounds.

METHODS

SAMPLE PREPARATION

YBa$_2$Cu$_3$O$_{6+x}$ single crystals were grown in non-reactive BaZrO$_3$ crucibles using a self-flux technique. The CuO$_x$-chain oxygen content was set to $x = 0.51$ by annealing in a flowing O$_2$:N$_2$ mixture and homogenized by further annealing in a sealed quartz ampoule, together with ceramic at the same oxygen content. After mounting for the cleave required in an ARPES measurement, the samples were cooled from 100 °C to room temperature over several days to establish the ortho-II superstructure ordering of the CuO$_x$-chain layer[28]. The particular sample used here was twinned, as confirmed by X-ray diffraction after the ARPES measurements.

ARPES EXPERIMENTS

ARPES measurements were carried out on the Electronic Structure Factory endstation at Beamline 7.01 of the Advanced Light Source. The data were measured with linearly polarized 110 eV photons and a Scienta R4000 electron analyser in angle-resolved mode. YBCO6.5 single crystals were cleaved *in situ* at a base pressure better than 2.5×10^{-11} torr and then oriented by taking fast Fermi surface scans. Several procedures were tried on these samples in an attempt to suppress the surface contribution to the total photoemission intensity and gain direct insight into the bulk electronic structure. For instance, samples were temperature-cycled between 20 and 100 K or were cleaved at higher temperature (~80 K) and then cooled to 20 K (ref. 29), to age and/or vary the characteristics of the cleaved surfaces. Whereas both procedures have proved successful in measuring the bulk dispersion and Fermi surface of layered Sr$_2$RuO$_4$ (ref. 29), no effect was observed in the case of YBCO6.5. Successful control of the self-doping of the cleaved surfaces was achieved by *in situ* deposition of submonolayers of potassium, with a commercial SAES getter source[30], on freshly cleaved YBCO6.5. In this last case, the samples were kept at 20 K at all times during the cleaving, K-deposition and ARPES measurements (temperature-dependent measurements could not be carried out because of the need to maintain the most stable experimental conditions over extended time, during and between subsequent K evaporations). All ARPES data shown in Figs 2–4 were obtained on the same sample, that is, as-cleaved, and after two subsequent K evaporations. Energy and angular resolutions were set to ~ 30 meV and 0.2° (±15° angular window) for the data in Figs 2 and 3, and to ~ 30 meV and 0.1° (±7° angular window) for the higher-quality Fermi surface mappings in Fig. 4. The Fermi surface maps of Figs 2 and 4 were obtained by integrating the ARPES intensity over a 30 meV energy window about E_F, and then by normalizing the intensity maps relative to one another for display purposes. A more quantitative comparison of the ARPES intensity for as-cleaved and K-deposited surfaces is given in the Supplementary Information on the basis of the analysis of momentum-distribution curves, which shows an overall intensity suppression by a factor of 4.4 and 7.2 for low and high K coverage, with respect to the as-cleaved surface.

References

1. Hussey, N. E., Abdel-Jawad, M., Carrington, A., Mackenzie, A. P. & Balicas, L. A coherent three-dimensional Fermi surface in a high-transition-temperature superconductor. *Nature* **425**, 814–817 (2003).
2. Platé, M. *et al*. Fermi surface and quasiparticle excitations of overdoped Tl$_2$Ba$_2$CuO$_{6+\delta}$ by ARPES. *Phys. Rev. Lett.* **95**, 077001 (2005).

3. Peets, D. C. *et al.* Tl$_2$Ba$_2$CuO$_{6+\delta}$ brings spectroscopic probes deep into the overdoped regime of the high-T_c cuprates. *New J. Phys.* **9**, 1–32 (2007).

4. Norman, M. R. *et al.* Destruction of the Fermi surface in underdoped high-T_c superconductors. *Nature* **392**, 157–160 (1998).

5. Kanigel, A. *et al.* Evolution of the pseudogap from Fermi arcs to the nodal liquid. *Nature Phys.* **2**, 447–451 (2006).

6. Shen, K. M. *et al.* Nodal quasiparticles and antinodal charge ordering in Ca$_{2-x}$Na$_x$CuO$_2$Cl$_2$. *Science* **307**, 901–904 (2005).

7. Doiron-Leyraud, N. *et al.* Quantum oscillations and the Fermi surface in an underdoped high-T_c superconductor. *Nature* **447**, 565–568 (2007).

8. Balakirev, F. F. *et al.* Fermi surface reconstruction at optimum doping in high-T_c superconductors. Preprint at <http://arxiv.org/abs/0710.4612> (2007).

9. LeBoeuf, D. *et al.* Electron pockets in the Fermi surface of hole-doped high-T_c superconductors. *Nature* **450**, 533–536 (2007).

10. Jaudet, C. *et al.* de Haas-van Alphen oscillations in the underdoped cuprate YBa$_2$Cu$_3$O$_{6.5}$. *Phys. Rev. Lett.* **100**, 187005 (2008).

11. Elfimov, I. S., Sawatzky, G. A. & Damascelli, A. Fermi pockets and correlation effects in underdoped YBa$_2$Cu$_3$O$_{6.5}$. *Phys. Rev. B* **77**, 060504(R) (2008).

12. Carrington, A. & Yelland, E. A. Band-structure calculations of Fermi-surface pockets in ortho-II YBa$_2$Cu$_3$O$_{6.5}$. *Phys. Rev. B* **76**, 140508(R) (2007).

13. Harrison, N., McDonald, R. D. & Singleton, J. Cuprate Fermi orbits and Fermi arcs: The effect of short-range antiferromagnetic order. *Phys. Rev. Lett.* **99**, 206406 (2007).

14. Chen, W.-Q., Yang, K.-Y., Rice, T. M. & Zhang, F. C. Quantum oscillations in magnetic field induced antiferromagnetic phase of underdoped cuprates : Application to ortho-II YBa$_2$Cu$_3$O$_{6.5}$. *Europhys. Lett.* **82**, 17004 (2008).

15. Millis, A. J. & Norman, M. Antiphase stripe order as the origin of electron pockets observed in 1/8-hole-doped cuprates. *Phys. Rev. B* **76**, 220503(R) (2007).

16. Chakravarty, S. & Kee, H.-Y. Fermi pockets and quantum oscillations of the Hall coefficient in high temperature superconductors. Preprint at <http://arxiv.org/abs/0710.0608> (2007).

17. Alexandrov, A. S. Theory of quantum magneto-oscillations in underdoped cuprate superconductors. *J. Phys. Condens. Matter* **20**, 192202 (2008).

18. Melikyan, A. & Vafek, O. Quantum oscillations in the mixed state of d-wave superconductor. Preprint at <http://arxiv.org/abs/0711.0776> (2007).

19. Schabel, M. C. *et al.* Angle-resolved photoemission on untwinned YBa$_2$Cu$_3$O$_{6.95}$. I. Electronic structure and dispersion relations of surface and bulk bands. *Phys. Rev. B* **57**, 6090–6106 (1998).

20. Lu, D. H. *et al.* Superconducting gap and strong in-plane anisotropy in untwinned YBa$_2$Cu$_3$O$_{7-\delta}$. *Phys. Rev. Lett.* **86**, 4370–4373 (2001).

21. Zabolotnyy, V. B. *et al.* Momentum and temperature dependence of renormalization effects in the high-temperature superconductor YBa$_2$Cu$_3$O$_{7-\delta}$. *Phys. Rev. B* **76**, 064519 (2007).

22. Derro, D. J. *et al.* Nanoscale one-dimensional scattering resonances in the CuO chains of YBa$_2$Cu$_3$O$_{6+x}$. *Phys. Rev. Lett.* **88**, 097002 (2002).

23. Liang, R., Bonn, D. A. & Hardy, W. N. Evaluation of CuO$_2$ plane hole doping in YBa$_2$Cu$_3$O$_{6+x}$ single crystals. *Phys. Rev. B* **73**, 180505 (2006).

24. Kondo, T. *et al.* Dual character of the electronic structure of YBa$_2$Cu$_4$O$_8$: The conduction bands of CuO$_2$ planes and CuO chains. *Phys. Rev. Lett.* **98**, 157002 (2007).

25. Hesper, R., Tjeng, L. H., Heeres, A. & Sawatzky, G. A. Photoemission evidence of electronic stabilization of polar surfaces in K$_3$C$_{60}$. *Phys. Rev. B* **62**, 16046–16055 (2000).

26. Sushkov, O. P., Sawatzky, G. A., Eder, R. & Eskes, H. Hole photoproduction in insulating copper oxide. *Phys. Rev. B* **56**, 11769–11776 (1997).

27. Eskes, H. & Eder, R. Hubbard model versus t–J model: The one-particle spectrum. *Phys. Rev. B* **54**, 14226–14229 (1996).

28. Liang, R., Bonn, D. A. & Hardy, W. N. Preparation and x-ray characterization of highly ordered ortho-II phase YBa$_2$Cu$_3$O$_{6.50}$ single crystals. *Physica C* **336**, 57–62 (2000).

29. Damascelli, A. *et al.* Fermi surface, surface states, and surface reconstruction in Sr$_2$RuO$_4$. *Phys. Rev. Lett.* **85**, 5194–5197 (2000).

30. Ohta, T., Bostwick, A., Seyller, T., Horn, K. & Rotenberg, E. Controlling the electronic structure of bilayer graphene. *Science* **313**, 951–954 (2006).

Author information
Reprints and permission information is available online at http://npg.nature.com/reprintsandpermissions. Correspondence and requests for materials should be addressed to A.D.